Experimental and Numerical Study on Mixed Mode I/II Fatigue Crack Growth in Planar Specimens

I. Varfolomeev[1], M. Burdack[1], S. Moroz[1], D. Siegele[1] and K. Kadau[2]

[1] Fraunhofer Institute for Mechanics of Materials IWM, Wöhlerstr. 11, 79111 Freiburg, Germany, E-mail: igor.varfolomeev@iwm.fraunhofer.de
[2] Siemens AG, Energy Sector, Mellinghofer Str. 55, 45473 Mülheim, Germany

ABSTRACT. *This paper focuses on the evaluation of predictive methods for the analysis of fatigue crack growth (FCG) under mixed mode I/II loading. The experimental part of the study consists of a series of fatigue crack growth tests performed on bend and tension specimens with geometries similar to the standard SE(B) and SE(T) ones. For the above specimen types, both mode I and mixed mode FCG tests are first performed. To facilitate an accurate evaluation of the mixed mode test results, finite element analyses of stress intensity factors for crack geometries following the experimentally measured trajectories are carried out. Additionally, the XFEM based algorithm available in the finite element code ABAQUS is explored with respect to its performance in predicting crack growth paths.*

The subsequent test evaluation focuses on examining a correlation between FCG rates for mixed mode loading conditions with the mode I baseline curve. The results suggest that, using mode I experimental data along with a mode I specimen analysis, both conservative and non-conservative prediction of mixed mode fatigue crack growth is possible. In this context recommendations of failure assessment procedures regarding the flaw re-characterisation and projection onto principal stress planes, as well rules for the transferability of mode I FCG curves to mixed mode conditions are discussed.

INTRODUCTION

Cracks initiated in components subject to multi-axial stress state, in welds, or flaws originated at manufacturing defects in forged or cast components, which are originally randomly oriented, can reveal some amount of mixed mode growth prior to become aligned with one of the principal stress planes. The assessment of such defects, including fatigue crack propagation, may follow rules established in fracture mechanics guidelines, e.g. [1-4]. The latter provide recommendations with respect to the alignment of mixed mode defects by their rotation or projection onto principal stress planes, the definition of an effective crack size [4] or an equivalent crack driving force [3, 5], whereas subsequent calculation procedures essentially rely on material data derived from mode I crack tests.

Comprehensive surveys of theoretical approaches, experimental techniques and examples of predicting fatigue crack growth (FCG) under mixed mode conditions can be found elsewhere, e.g. [5-7]. In particular, numerous investigations have been devoted

to establish criteria and solutions for determining the crack propagation angle in mixed mode, as well as to develop numerical techniques for simulating crack growth in complex structural components and stress fields [8-10]. Inherently or by definition, most calculation models for mixed mode cracks incorporate mode I FCG curves along with an equivalent stress intensity factor as the crack driving force parameter. Validation of such a procedure requires experimental data for both mode I and mixed mode loading conditions, whereas respective tests are rather scarce, see e.g. [11, 12].

In this paper FCG tests are performed on bend and tension specimens representative of mode I and mixed mode I/II geometries. Based on the experimental results and finite element analyses of stress intensity factors for the respective specimen and crack geometries, FCG rates at mixed mode loading conditions are evaluated with respect to the mode I baseline. The results show that, using mode I experimental data along with a mode I specimen analysis, both conservative and non-conservative prediction of mixed mode fatigue crack growth is possible. To explore the performance of alternative analysis methods, the XFEM [10] algorithm implemented in ABAQUS [13] is applied for calculating crack growth paths.

TEST DESCRIPTION

The material considered in this study is a high strength steel for high temperature applications. The geometries of the test specimens are shown in Figure 1. All specimens are 240 mm long, with a test cross-section of $W \times B = 40 \times 20$ mm² for SE(B) and $W \times B = 40 \times 10$ mm² for SE(T) geometries. Altogether eight SE(B) and four SE(T) specimens were tested.

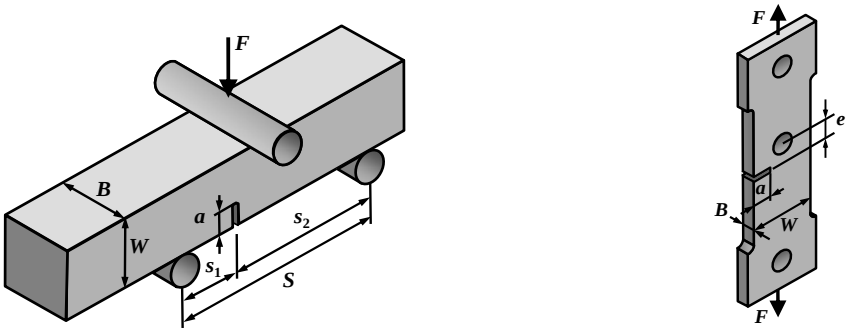

Figure 1. Schematic of SE(B) and SE(T) specimens adopted.

When preparing the specimens, an initial edge notch of a 4 mm depth was first introduced by spark erosion. In all but 4 SE(B) specimens the initial notches are located at the specimen centre, i.e. a distance of 120 mm from the specimen ends. In the remaining four SE(B) specimens the initial notch is located 40 mm from the specimen centre. Fatigue pre-cracking up to the crack depth of about 6 mm was accomplished under pure mode I cyclic loading.

To minimize load interaction and related crack closure effects on fatigue crack propagation, all subsequent tests of SE(B) specimens were carried out at a constant load amplitude. With increasing FCG rates, the final phase of testing for some specimens, as

well as the whole testing for SEB2 was performed in a servo-hydraulic machine at a frequency of 5 Hz. In contrast, all SE(T) specimens were tested in the resonant testing machine at a frequency of about 110 Hz, at gradually decreasing load amplitude to attain moderate crack growth rates. Both fatigue pre-cracking and crack growth tests were performed at the load ratio of $R = 0.1$, at room temperature.

Table 1. Geometrical parameters and test conditions for SE(B) specimens

Loading mode	Specimen, test phase	a_{min} … a_{max} mm	Frequency Hz	Span parameters, mm			Upper load, kN	Nominal tensile stress, MPa
				S	s_1	s_2		
I	SEB1	6…24	110	160	80	80	12	90
	SEB2	6…24	5				36	270
	SEB3	6…10 / 10…27.5	110 / 5				24	180
I+II	SEB5	6…18.7 / 18.7…30.5	110 / 5	160	40	120	24	90
	SEB6	6…12.1 / 12.1…26.5	110 / 5				36	135
	SEB7	6…26.2	5				48	180
I+II (2 stages)	SEB4 / 1	6…12.6	110	120	30	90	32	90
	SEB4 / 2	12.6…23.5	110	80	40	40	36	135
	SEB8 / 1	6…12.5	110	160	40	120	24	90
	SEB8 / 2	12.5…26	110	80	40	40	24	90

Table 2: Geometrical parameters and test conditions for SE(T) specimens

Loading mode	Specimen	a_{min} … a_{max} mm	Frequency Hz	Hole parameters, mm		Upper load, kN (gradually decreasing)	Nominal tensile stress, MPa
				Ø	e		
I+II	SET1	6.1…30.6	110	10	10	24.6 → 10.6	61.5 → 26.5
	SET2	6.1…29.9	110	10	10		
	SET3	6…30	110	10	8		
I	SET4	6…25	110	-	-	26 → 10	65 → 25

Both SE(B) and SE(T) specimens shown in Figure 1 allow for testing at mode I and mixed mode loading conditions. Three bend specimens referred to as SEB1, SEB2 and SEB3 were tested under pure mode I loading with symmetrically positioned supporting rollers ($s_1 = s_2 = 80$ mm). Further three specimens denoted as SEB5, SEB6 and SEB7 were subject to mixed mode loading by asymmetrically placing the lower rollers with the span values equal to $S = s_1 + s_2 = 160$ mm and $s_2/s_1 = 3$. Two additional specimens, SEB4 and SEB8, were tested following two consequent steps: first, asymmetric loading with $s_2/s_1 = 3$ was applied up to a crack depth of some 12.5 mm proceeded by symmetrical loading of a resulting curved crack at $s_1 = s_2 = 40$ mm.

Mixed mode loading for the SE(T) specimens was achieved by machining a hole of 10 mm diameter in the central part of the specimens after pre-cracking, similar to the approach in [12]. The hole was centred with respect to the specimen width but shifted some distance with respect to the original crack plane. The eccentricity parameter e, i.e. the distance from the hole centre to the pre-crack plane, was equal to $e = 10$ mm for the specimens SET1 and SET2, and $e = 8$ mm for the specimen SET3, respectively. Additionally, one specimen without hole drilling, denoted as SET4, was tested under pure mode I conditions.

Geometrical parameters and loading conditions for the bend and tension specimens considered in this study are summarized in Table 1 and Table 2, respectively. Note that throughout the paper the crack size a represents the projection of the crack path on the initial pre-crack plane.

Crack Paths in Mixed Mode Specimens

Figure 2a,b shows crack growth paths in two mixed mode bend specimens SEB5 and SEB4. Note different crack propagation behaviour for the former specimen tested at a fixed position of the supporting rollers, as compared to the SEB4 specimen for which a two-stage loading procedure was adopted. For the latter specimen, the initial phase of crack growth from some 6 mm to 12.5 mm depth is governed by asymmetrically applied bending load, similar to loading conditions for SEB5. In the second phase the SEB4 specimen is loaded symmetrically with respect to the initial crack plane, thus resulting in crack kinking towards the symmetry plane.

Crack trajectories for the SE(T) specimens are depicted in Figure 2c,d. Characteristic for the SET1 and SET2 specimens in which the hole centre is located 10 mm from the pre-crack plane is the initial growth direction towards the bore with considerable retardation at the bore boundary where crack branching partially took place. Finally, after some 50,000 (SET1) to 200,000 (SET2) load cycles, further crack propagation from the bore backwards was observed. In case of the specimen SET3 with the hole centre located 8 mm from the pre-crack plane, the crack continuously propagated towards the bore and finally broke the ligament.

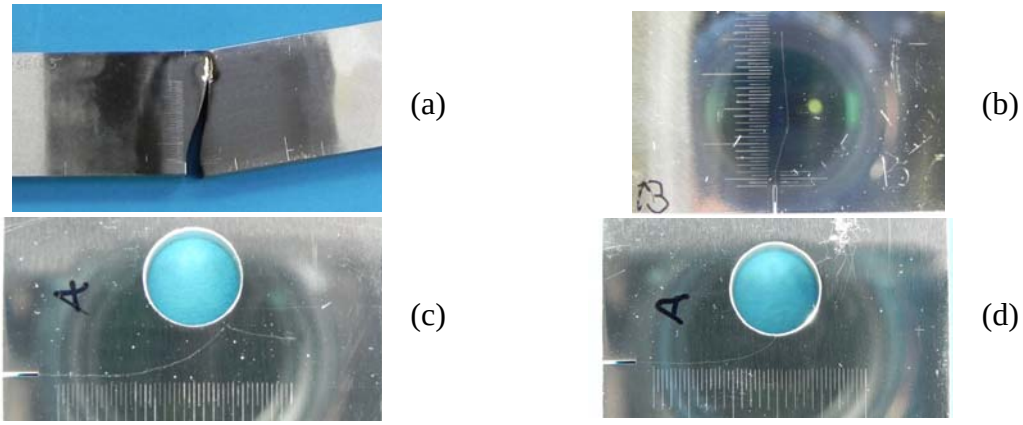

Figure 2. Crack paths: a) SEB5; b) SEB4; c) SET1, e = 10 mm; d) SET3, e = 8 mm.

NUMERICAL ANALYSES

Estimation of Stress Intensity Factors

The stress intensity factors at mixed mode loading conditions were numerically calculated using the finite-element (FE) code ABAQUS [13], based on experimentally measured crack paths. Altogether 30 FE models were established representative of different crack sizes and four specimens groups: 1) SEB5, SEB6, SEB7; 2) SEB4, SEB8; 3) SET1, SET2; 4) SET3. The crack path in each model followed a trajectory obtained by averaging measurements for all specimens in the respective group. The analyses were carried out assuming elastic material behaviour, taking into account the contact interaction of the SE(B) specimen with the supporting rollers or the SE(T) specimen with loading pins.

The calculated K_I and K_{II} values are normalized with respect to the crack size, a, and a nominal normal stress acting at the crack mouth location in an uncracked specimen. The nominal bending and tensile stresses are given by (see notations in Figure 1)

$$\sigma_b = \frac{6M(x=0)}{BW^2} = \frac{3Fs_1}{BW^2}, \quad \sigma_m = \frac{F}{BW} \tag{1}$$

for the SE(B) and SE(T) specimens, respectively. In Eq. (1) the coordinate $x = 0$ indicates the horizontal position of the initial notch (crack mouth) in the SE(B) specimen. The respective dimensionless stress intensity factors for both mode I and mode II are expressed as follows

$$F_{I,II} = \frac{K_{I,II}}{\sigma_b\sqrt{\pi a}}, \quad F_{I,II} = \frac{K_{I,II}}{\sigma_m\sqrt{\pi a}} \tag{2}$$

for the SE(B) and SE(T) specimens, respectively.

The numerical results in Figure 3 demonstrate that mode I loading dominates the crack propagation behaviour. For the SE(B) specimens, the mode II stress intensity factor is almost zero, except for the very beginning stage of crack growth starting from the mode I pre-crack, as well as at shifting from the asymmetric to symmetric roller position for the specimens SEB4 and SEB8. Besides, the final stage of crack growth prior fracture is also influenced by mode II. Similar conclusions hold for the SE(T) specimens which show a moderate increase of mode II crack tip loading either for deep cracks of $a/W > 0.7$ (SET1, SET2) or at the onset of ligament break through (crack running in the bore in the SET3 specimen).

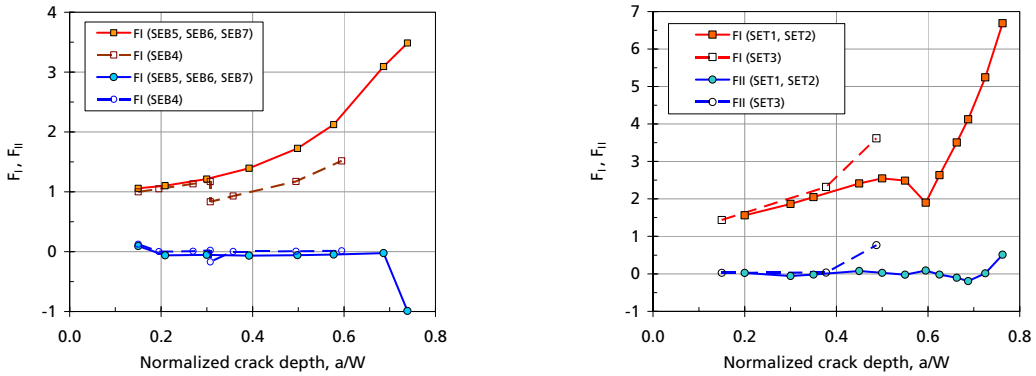

(a) SE(B) (b) SE(T)

Figure 3. Dimensionless stress intensity factors for mixed mode specimens.

In all cases considered, except for the deepest crack in bend specimens, the absolute ratio of mode II to mode I stress intensity factor, K_{II}/K_I, is well below 0.2. Assuming an equivalent stress intensity factor range according to [5]

$$\Delta K_{eq} = \frac{\Delta K_I}{2} + \frac{1}{2}\sqrt{\Delta K_I^2 + 5.34\Delta K_{II}^2}\,, \tag{3}$$

the contribution of mode II loading to the crack driving force does not exceed 5%, so that the test evaluation performed below is based on the mode I stress intensity factor.

Simulation of Crack Growth Paths

As the XFEM approach [10] is receiving an increasing interest in fracture mechanics applications, this numerical algorithm available in ABAQUS [13] is applied below to simulate FCG paths for the asymmetrically loaded bend specimens (SEB5, SEB6 and SEB7), as well as for the SE(T) configurations denoted by SET1 and SET3. The SE(B) model was meshed using square-shaped elements with the element size of 1 mm. For the SE(T) models two mesh types – square-shaped and randomly shaped elements (referred in Figure 4 to as "regular" and "irregular" mesh, respectively) – both having the element size below 0.5 mm were employed.

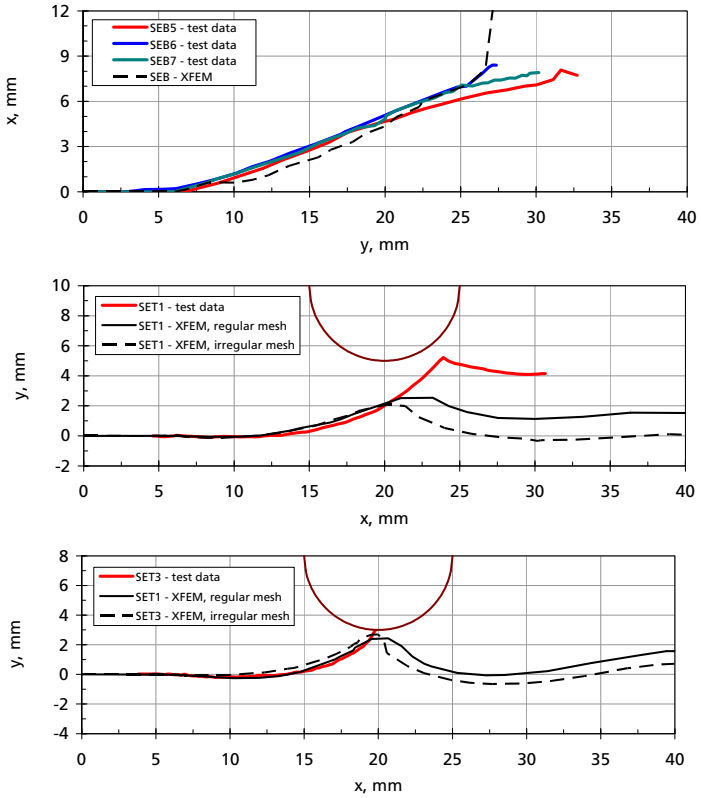

(a) SE(B)

(b) SE(T), e = 10 mm

(c) SE(T), e = 8 mm

Figure 4. Calculated vs. measured crack growth paths.

The calculated and experimental crack paths are compared in Figure 4. One can sum up that a fairly good agreement exists between the numerical and test results for the SE(B) and SET3 specimens. In the latter case, the XFEM analysis is able of predicting crack propagation towards the bore, although it cannot describe the specimen's fracture behaviour. At the same time a considerable discrepancy is noticed for the SET1 specimen, suggesting that crack growth mechanisms are not properly captured by fracture criteria currently implemented in [13].

EVALUATION OF FCG TESTS

Figure 5 summarizes the experimental and numerical results for all mixed mode specimens considered. The diagrams show FCG rates, normalized with respect to the mode I baseline, as a function of ΔK_I. All test results correspond to the Paris range of the FCG diagram. The mode I baseline is obtained as a 50% probability curve approximating FCG data for the specimens SEB1, SEB2, SEB3 and SET4.

In Figure 5a test data obtained at high and low load frequencies are shown separately as filled and open symbols, respectively. One can conclude that, with a few exceptions, at a high frequency FCG rates at mixed mode are below those at pure mode I. However, the reverse trend is observed at a low frequency and higher stress intensity factors. As the load frequency correlates with the strain rate and hence with the crack tip plasticity, the later may be assumed to influence the crack propagation behaviour.

Figure 5b suggests that FCG rates for mixed mode tension specimens tend to be higher than in mode I. The difference between mixed mode FCG rates and the mode I baseline is especially pronounced for the crack depth of about 16 to 24 mm (SET1 and SET2) or 18 to 20 mm (SET3), when the crack tip rapidly approaches the bore. The respective data points are indicated in Figure 5b by open circles.

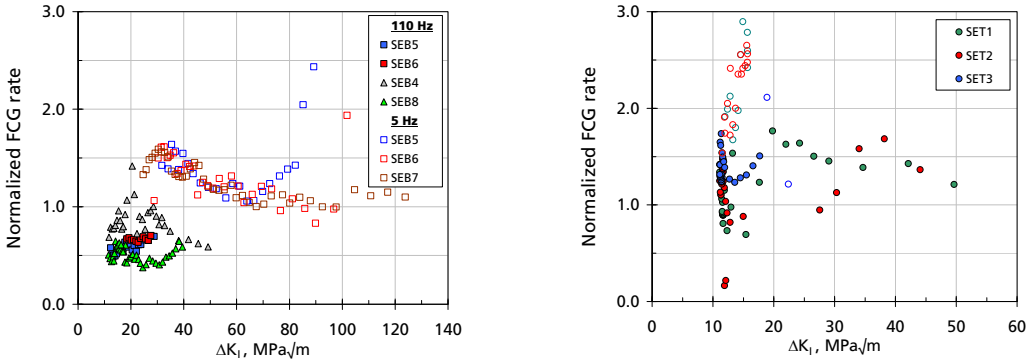

a) SE(B) specimens b) SE(T) specimens

Figure 5. Mixed mode FCG rates normalized with respect to the mode I baseline.

CONCLUSIONS

The results of this paper demonstrate that no distinct correlation between mode I and mixed mode FCG rates can be established based on conventional analysis approaches. When using mode I FCG curves along with mode I stress intensity factor analysis, both conservative (bend specimens, high frequency) and non-conservative (SE(T) specimens, SE(B) specimens at low frequency) prediction of crack growth rates can be achieved.

No significant alteration of the results is achieved by applying the projection or rotation rules [1-3], or by correcting the crack size according to [4]. At least for the specimen geometries considered above, such procedures would insignificantly increase the effective crack size and thus the crack driving force. In this respect it should be noted that the assessment rules [1-4] for mixed mode cracks are scarcely applicable to

the test conditions realized in this study, especially when non-uniformly distributed stresses act along the prospective crack line or the principal stress changes its direction along the crack trajectory.

Finally, some test conditions (stress or ΔK level, load frequency) seem to additionally influence FCG rates, both in mode I and mixed mode. These observations, though not explicitly addressed in this paper, are consistent with some studies on constraint and crack tip plasticity effects on fatigue crack growth behaviour, see e.g. [12, 14-17].

PERMISSION FOR USE STATEMENT

REFERENCES

1. Assessment of the Integrity of Structures Containing Defects (2007). R6 Revision 4, British Energy Generation Ltd.
2. FITNET: Fitness-for-Service Procedure (2008). M. Kocak, et al. (Eds.), GKSS Research Center Geesthacht.
3. Fracture Mechanics Proof of Strength for Engineering Components (2009). FKM Guideline, 3rd revised edition, VDMA Publ., Frankfurt.
4. Fitness-For-Service, API 579-1 / ASME FFS-1 Procedure (2007). American Society of Mechanical Engineers/ American Petroleum Institute, API 579, 2nd edition.
5. Richard, H.A. (2003). *Materialprüfung* **45**, 513-518.
6. Sih, G.C. (1973). In: *Mechanics of Fracture*, Vol. 2, pp. XXI-XLV, Sih, G.C. (Ed.), Noordhoff Int. Publ., Leyden, The Netherlands.
7. Qian, J., Fatemi, A., (1996). *Eng. Fract. Mech.* **55**, 969-990.
8. Bremberg, D., Dhondt, G. (2009). In: *Crack Paths 2009*, Vicenza.
9. Schöllmann, M., Fulland, M., Richard, H.A. (2003). *Eng. Fract. Mech.* **70**, 249-268.
10. Belytschko, T., Black, T. (1999). *Int J. Num. Meth. Eng*. **45**, 601-620.
11. Borrego, L.P., Antunes, F.V., Costa, J.M., Ferreira, J.M. (2006). *Int. J. Fatigue* **28**, 618-626.
12. Seitl, S., Knésl, Z. (2008). *Eng. Fract. Mech.* **75**, 857-865.
13. ABAQUS, Version 6.11 (2011). Dassault Systèmes Simulia Corp., Providence, RI.
14. Vecchio, R.S., Crompton, J.S., Hertzberg, R.W. (1987). *Fatigue Fract. Eng. Mat. Struct*. **10**, 333-342.
15. Tong, J. (2002). *Eng. Fract. Mech*. **69**, 1325-1337.
16. Hutar, P., Seitl, S., Knésl, Z. (2006). *Comp. Mat. Sci*. **37**, 51-57.
17. Varfolomeev, I., Luke, M., Burdack, M. (2011). *Eng. Fract. Mech*. **78**, 742-753.